PERGAMON

Journal of Quantitative Spectroscopy & Radiative Transfer 79–80 (2003) 911–920

Journal of Quantitative Spectroscopy & Radiative Transfer

www.elsevier.com/locate/jqsrt

Scattering matrix of quartz aerosols: comparison and synthesis of laboratory and Lorenz–Mie results

Li Liu[a,b], Michael I. Mishchenko[b,*], Joop W. Hovenier[c,d], Hester Volten[d,e], Olga Muñoz[f]

[a] *Department of Earth and Environmental Sciences, Columbia University, 2880 Broadway, New York, NY 10025, USA*

[b] *NASA Goddard Institute for Space Studies, 2880 Broadway, New York, NY 10025, USA*

[c] *Department of Physics and Astronomy, Free University, De Boelelaan 1081, 1081 HV Amsterdam, The Netherlands*

[d] *Astronomical Institute "Anton Pannekoek", University of Amsterdam, Kruislaan 403, 1098 SJ Amsterdam, The Netherlands*

[e] *FOM-Institute for Atomic and Molecular Physics, Kruislaan 407, 1098 SJ Amsterdam, The Netherlands*

[f] *Instituto de Astrofisica de Andalucia, P.O. Box 3004, Granada 18080, Spain*

Received 3 May 2002; accepted 18 August 2002

Abstract

This paper compares and combines the results of laboratory measurements of the Stokes scattering matrix for nonspherical quartz aerosols at a visible wavelength in the scattering angle range 5–173° and the results of Lorenz–Mie computations for projected-area-equivalent spheres with the refractive index of quartz. A synthetic normalized phase function is constructed based on the laboratory data and the assumption that the diffraction forward-scattering peak is the same for spherical and nonspherical projected-area-equivalent particles. The experimental scattering matrix for the nonspherical quartz particles is poorly represented by the Lorenz–Mie results for most scattering angles. However, the asymmetry parameters for the synthetic phase function and for the equivalent spherical particles are similar.

Keywords: Electromagnetic scattering; Nonspherical particles; Polarization

1. Introduction

Particle nonsphericity has been shown to be an important factor that must be carefully addressed in optical characterization of mineral atmospheric aerosols [1–4]. Despite the significant recent progress

* Corresponding author. Tel.: +1-212-678-5590; fax: +1-212-678-5622.
E-mail address: crmim@giss.nasa.gov (M.I. Mishchenko).

0022-4073/03/$ - see front matter © 2003 Elsevier Science Ltd. All rights reserved.
doi:10.1016/S0022-4073(02)00328-X

[5–9], theoretical and numerical techniques are still limited in their ability to simulate electromagnetic scattering by realistic polydispersions of irregular particles. Therefore, laboratory measurement techniques [10,11] remain an important source of information on scattering properties of nonspherical aerosols.

In a recent paper, Volten et al. [12] presented an extensive dataset which includes the results of laboratory measurements in the visible of the Stokes scattering matrix in a wide scattering angle range for several types of polydisperse, randomly oriented mineral aerosols and accompanying size distribution data. A traditional limitation of such laboratory measurements is the lack of data at very small and very large scattering angles (in this case, from 0° to 5° and from 173° to 180°), which precludes the determination of the absolute angular dependence of the phase function $a_1(\Theta)$ by using the standard normalization condition,

$$\frac{1}{2}\int_0^{\pi} \mathrm{d}\Theta \sin\Theta a_1(\Theta) = 1, \tag{1}$$

where Θ is the scattering angle. As a consequence, Volten et al. plotted the relative quantity $\tilde{a}_1(\Theta) = a_1(\Theta)/a_1(30^\circ)$ rather than $a_1(\Theta)$, which makes their measurements less useful in those cases when the absolute phase function values are needed [1–4,13].

The main purpose of this paper is to explore what insight and knowledge can be gained by comparing and synthesizing an experimental and a theoretical scattering matrix in the visible part of the spectrum. A unique opportunity to do so was provided by a sample of randomly oriented quartz particles, because (i) its scattering matrix at a wavelength of 441.6 nm was measured in the laboratory over a wide range of scattering angles [12]; (ii) independently measured size distribution data are available for this sample [12]; and (iii) independently measured values of the refractive index of quartz at visible wavelengths are also available [14]. Consequently, in this case the experimental scattering matrix can be contrasted with the most physically relevant theoretical Lorenz–Mie scattering matrix, namely the one that is valid for projected-area-equivalent spheres with the same refractive index.

The organization of this paper is as follows. First, we parallel the laboratory study of Volten et al. [12] for the quartz particle sample by performing theoretical Lorenz–Mie computations for projected-area-equivalent quartz spheres. Second, we construct a synthetic phase function for the quartz particle sample using the relative angular profile of the phase function measured by Volten et al., assuming that the forward-scattering diffraction peak is independent of the particle shape and depends only on the distribution of surface-equivalent-sphere radii, and using the normalization condition of Eq. (1). The synthetic phase function is then used to compute the corresponding value of the asymmetry parameter,

$$\langle \cos\Theta \rangle = \frac{1}{2}\int_0^{\pi} \mathrm{d}\Theta \sin\Theta a_1(\Theta)\cos\Theta. \tag{2}$$

Finally, we briefly compare all elements of the scattering matrix and the asymmetry parameter for the quartz particle sample and for projected-area-equivalent quartz spheres.

2. Measurements and Lorenz–Mie computations

Volten et al. [12] used a laser particle sizer to measure the normalized projected area distribution $S(\log r)$ of the quartz particle sample, where $S(\log r)\mathrm{d}(\log r)$ is the fraction of the total projected area of the sample contributed by particles with radii in the size range from $\log r$ to $\log r + \mathrm{d}(\log r)$. The equivalent-sphere radius r of a nonspherical particle is defined as the radius of a sphere that has a projected area equal to the average projected area of the nonspherical particle in random orientation. This distribution was presented in tabular form by Volten [15] and is shown in Fig. 1. Note that equal areas under the curve correspond to equal contributions to the total projected area. The effective radius r_{eff} and effective variance v_{eff} of this broad size distribution are 2.3 μm and 2.4, respectively, where [16]

$$r_{\mathrm{eff}} = \frac{1}{\langle G\rangle}\int_{r_{\min}}^{r_{\max}} \mathrm{d}r\, n(r) r\pi r^2, \tag{3}$$

$$v_{\mathrm{eff}} = \frac{1}{\langle G\rangle r_{\mathrm{eff}}^2}\int_{r_{\min}}^{r_{\max}} \mathrm{d}r\, n(r)(r - r_{\mathrm{eff}})^2\pi r^2, \tag{4}$$

and

$$\langle G\rangle = \int_{r_{\min}}^{r_{\max}} \mathrm{d}r\, n(r)\pi r^2 \tag{5}$$

is the average area of the particle geometrical projection. Here $n(r)\,\mathrm{d}r$ is the fraction of projected-area-equivalent spheres with radii between r and $r + \mathrm{d}r$.

The open circles in Fig. 2 show the experimentally determined elements of the scattering matrix versus scattering angle at a wavelength of 441.6 nm. The measurements were performed at 5° intervals for scattering angles, Θ, in the range from 5° to 170° and at 1° intervals for Θ from 170° to 173°. The experimental phase function is normalized by its value at $\Theta = 30°$ and is plotted on a

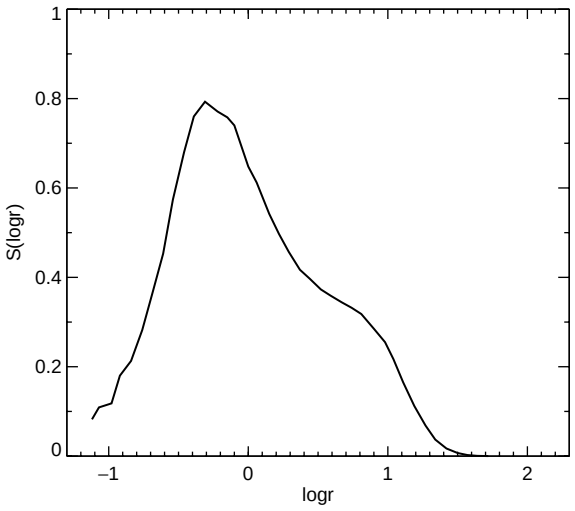

Fig. 1. Normalized distribution of the average area of the particle projection for randomly oriented quartz aerosols. Here r is expressed in micrometers.

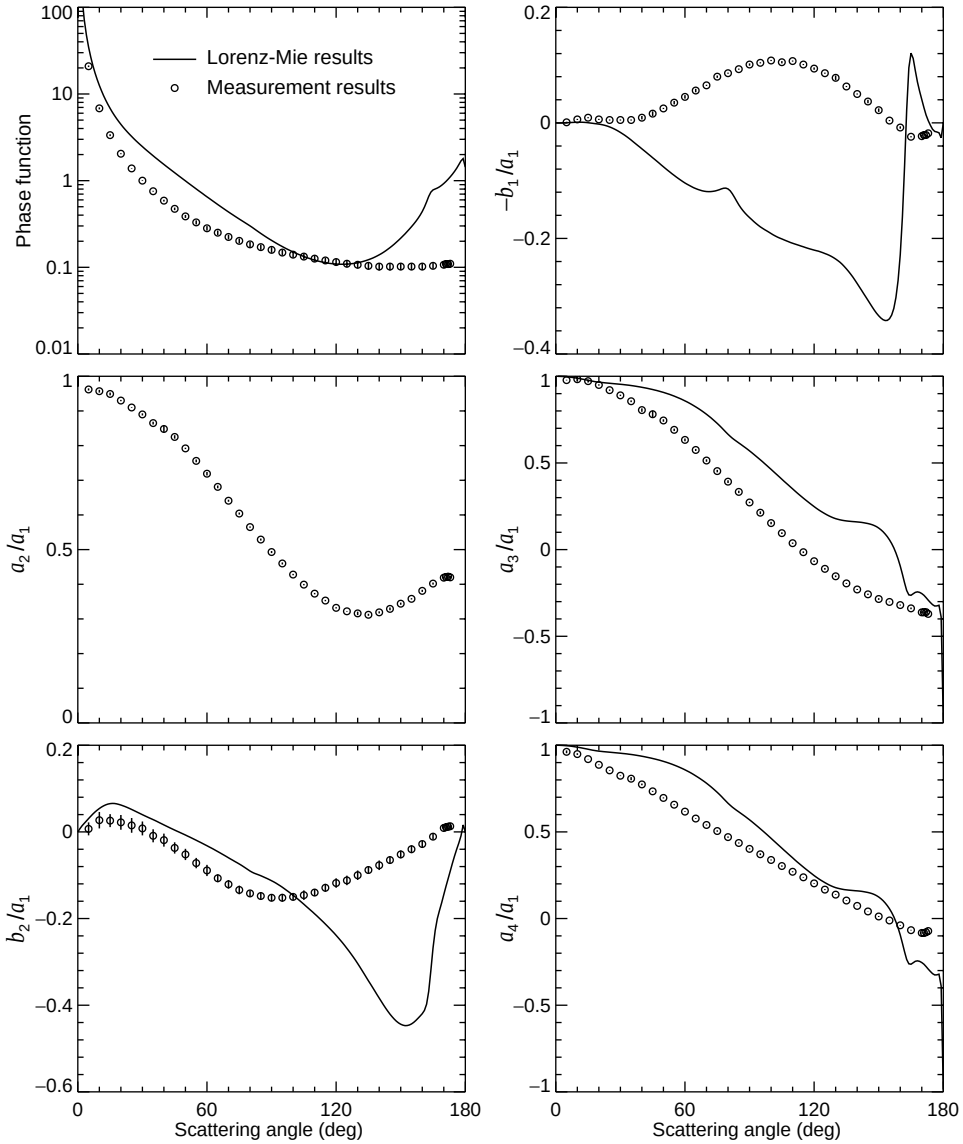

Fig. 2. Laboratory data for nonspherical quartz aerosols and results of Lorenz–Mie computations for projected-area-equivalent quartz spheres. Experimental errors are shown by vertical error bars.

logarithmic scale. The other elements are shown relative to the phase function. Within measurement errors, the scattering matrix has the standard block-diagonal form,

$$\begin{bmatrix} a_1(\Theta) & b_1(\Theta) & 0 & 0 \\ b_1(\Theta) & a_2(\Theta) & 0 & 0 \\ 0 & 0 & a_3(\Theta) & b_2(\Theta) \\ 0 & 0 & -b_2(\Theta) & a_4(\Theta) \end{bmatrix}, \tag{6}$$

thereby indicating that during the measurement, the quartz particles suspended in the air jet were randomly oriented and formed a macroscopically isotropic and mirror-symmetric scattering medium [17].

For comparison, the solid curves in Fig. 2 show the results for projected-area-equivalent spheres calculated with the Lorenz–Mie code described in [18] and available on the Internet at http://www.giss.nasa.gov/∼crmim. For these computations, we employed the number size distribution $n(r)$ derived from the measured projected area distribution shown in Fig. 1. Furthermore, we used the real part of the refractive index 1.559 as typical of quartz at wavelengths close to 440 nm [14]. Since quartz is essentially nonabsorbing at visible wavelengths, the imaginary part of the refractive index was set to zero. The theoretical Lorenz–Mie phase function is normalized according to Eq. (1). Note that Volten et al. [12] use the time factor $\exp(\mathrm{i}\omega t)$ rather than the factor $\exp(-\mathrm{i}\omega t)$ adopted in [18], which causes a sign difference in the numerical values of the ratio $b_2(\Theta)/a_1(\Theta)$. Therefore, the sign of the experimentally measured ratio $b_2(\Theta)/a_1(\Theta)$ in Fig. 2 is opposite to that in [12].

3. Synthetic phase function

As we have already mentioned, Volten et al. [12] measured the relative phase function $\tilde{a}_1(\Theta)$ rather than the actual phase function. Therefore, although the laboratory data give the relative angular profile of the phase function in the scattering angle interval from 5° to 173°, the exact vertical position of the experimental curve in (Θ, a_1) coordinates remains uncertain. The dashed and dot–dashed curves in Fig. 3 show two extreme vertical positions of the experimental curve intended to match the phase function values for nonspherical and projected-area-equivalent spherical quartz particles at side- and backscattering angles, respectively. It is seen that in both cases spherical-nonspherical phase function differences at other angles are very large and can exceed a factor of 10. Placing the experimental curve in an intermediate position minimizes the differences at side- and backscattering angles on average (dotted curve), but they can still exceed a factor of 3. It is thus clear that irrespective of the actual vertical position of the experimental curve, spherical-nonspherical phase function differences remain very large at specific scattering angles.

In order to get a better idea of a plausible vertical position of the phase function for nonspherical quartz particles, we did the following. It is known that the phase function at small scattering angles for particles greater than a wavelength is mostly determined by Fraunhofer diffraction and is largely the same for spherical and projected-area-equivalent nonspherical particles with moderate aspect ratios and regular shapes (e.g., [19,20]). Therefore, we used the results of Lorenz–Mie computations for projected-area-equivalent quartz spheres in the scattering angle interval from 0° to 5° and shifted the experimental $\tilde{a}_1(\Theta)$-curve in the vertical direction until its value at $\Theta = 5°$ matched the Lorenz–Mie result. Finally, the experimental phase function was extrapolated from $\Theta = 173°$ to 180° using cubic splines.

We then evaluated the left-hand-side of Eq. (1) in order to check whether this synthetic phase function satisfied the normalization condition. The result was 0.848 rather than the expected value unity. Since the contribution of the interval from $\Theta = 173°$ to 180° to the integral was only 0.005, it is obvious that the use of spline extrapolation could not explain the large discrepancy between the computed and expected integral values.

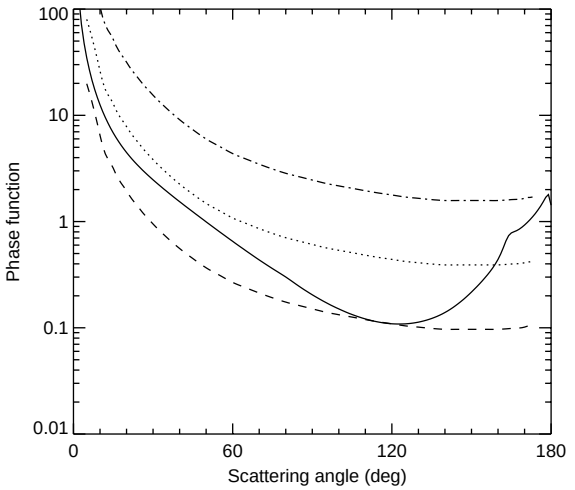

Fig. 3. The pattern of the differences between the Lorenz–Mie phase function for spherical quartz particles (solid curve) and the phase function for nonspherical quartz aerosols depends on the vertical position of the experimental $\tilde{a}_1(\Theta)$ profile (dashed, dotted, and dot–dashed curves).

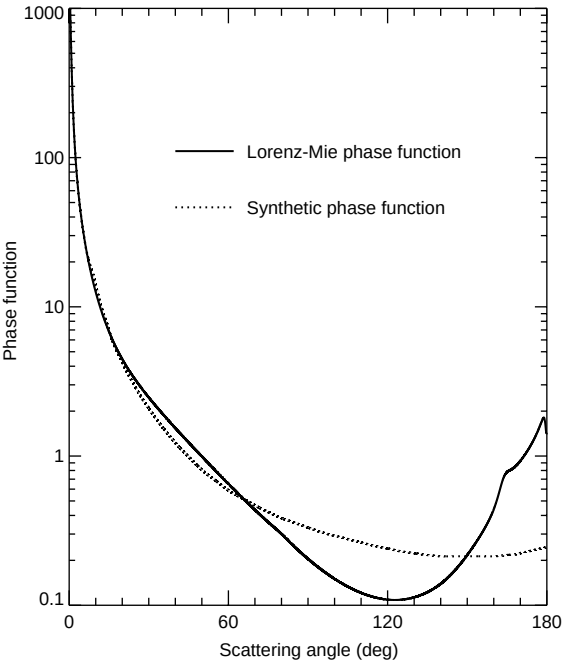

Fig. 4. Synthetic and Lorenz–Mie phase functions for randomly oriented nonspherical quartz aerosols and projected-area-equivalent quartz spheres, respectively.

There are several potential contributors to this discrepancy, including the following.

- Experimental errors. These are always a potential source of complications. However, in this case the errors (indicated by error bars in Fig. 2) appear to be too small to be a likely explanation of the above discrepancy.
- The possible inaccuracy of the underlying assumption, made on the basis of computations for regular nonspherical shapes, that the phase functions for projected-area-equivalent spherical and nonspherical particles are the same in the forward-scattering direction. One should not exclude the possibility that this assumption may not be sufficiently precise for the irregular (including complicated surface structure) quartz aerosols under consideration, especially at scattering angles as large as 5°.
- Inaccuracies in the measured size distribution of the quartz aerosols, especially for the smallest particles. For example, we have found that truncating the measured size distribution by leaving out all particles with equivalent-sphere radii smaller than 0.31 μm and then renormalizing the resulting size distribution improves the normalization of the synthetic phase function significantly. Therefore, we should not exclude the possibility that the size distribution of the quartz particles during the scattering matrix measurements contained fewer small particles than was deduced from the separate measurements with the particle sizer.

- Multiple scattering effects in the laboratory measurements. However, these appear to be very unlikely, since the shape of the curves for $\tilde{a}_1(\Theta)$ did not show any significant difference when the amount of scattering mineral aerosol particles was doubled (see also [21]).
- Some constructive interference of light singly scattered by particles in the forward direction [22] may have contributed to the intensity measured at small scattering angles.

Given these uncertainties, we have decided to use, as a tentative fix, the following simple procedure. Since it is likely that the most "vulnerable" quantity is the phase function at the smallest scattering angle, we kept changing the experimental $\tilde{a}_1(5^\circ)$ value in very small increments and repeated the process of compiling the synthetic phase function until it satisfied the normalization condition of Eq. (1) to better than 0.001. The result is shown in Fig. 4 by the dotted curve and is contrasted with the Lorenz–Mie phase function for projected-area-equivalent quartz spheres depicted by the solid curve. The respective asymmetry parameters evaluated using Eq. (2) are 0.669 and 0.698.

It is often convenient to represent a phase function by expanding it in Legendre polynomials $P_n(\cos\Theta)$ [17]:

$$a_1(\Theta) = \sum_{n=0}^{n_{\max}} \alpha_1^n P_n(\cos\Theta). \tag{7}$$

The expansion coefficients for the synthetic phase function were computed by evaluating numerically the integral in the formula

$$\alpha_1^n = (n + \tfrac{1}{2}) \int_0^\pi \mathrm{d}\Theta \sin\Theta a_1(\Theta) P_n(\cos\Theta) \tag{8}$$

and are available from the corresponding author upon request.

4. Discussion and conclusions

Fig. 4 represents the main result of this paper. It closely resembles Fig. 6(a) of Jaggard et al. [23] depicting experimental and theoretical Lorenz–Mie results for Raft River soil dust. In agreement with the results of Jaggard et al. and previous theoretical studies of light scattering by polydisperse, randomly oriented spheroids and circular cylinders [19,20], Fig. 4 reveals the following three distinct regions:

$$\text{nonsphere} < \text{sphere from } \Theta \sim 15^\circ\text{–}20^\circ \text{ to } \Theta \sim 65^\circ;$$

$$\text{nonsphere} \gg \text{sphere from } \Theta \sim 65^\circ \text{ to } \Theta \sim 150^\circ;$$

$$\text{nonsphere} \ll \text{sphere from } \Theta \sim 150^\circ \text{ to } \Theta = 180^\circ.$$

The asymmetry parameter for the nonspherical quartz particles, as determined from the synthetic phase function, is smaller than that for the projected-area-equivalent quartz spheres, but not by much, which also agrees well with theory [19,20].

The differences between the Lorenz–Mie and the synthetic phase function are quite significant: they can exceed a factor of two at side-scattering angles and are even greater in the backscattering

direction. Large differences between the experimental and Lorenz–Mie results also occur for all other scattering matrix elements (see Fig. 2) and follow the general pattern discussed by Mishchenko et al. [24]. Specifically, the degree of linear polarization for unpolarized incident light, $-b_1(\Theta)/a_1(\Theta)$, tends to be positive at side-scattering angles for the nonspherical particles, but shows a broad negative region at side-scattering angles and a narrow positive feature at $\Theta\sim165^\circ$ caused by the primary rainbow for the spherical aerosols. Whereas $a_2(\Theta)/a_1(\Theta) \equiv 1$ for spherically symmetric scatterers, the $a_2(\Theta)/a_1(\Theta)$ curve for the nonspherical quartz aerosols significantly deviates from unity and exhibits strong backscattering depolarization. Similarly, $a_3(\Theta)/a_1(\Theta) \equiv a_4(\Theta)/a_1(\Theta)$ for spherically symmetric particles, whereas $a_4(\Theta)/a_1(\Theta)$ for the nonspherical quartz aerosols tends to be significantly greater than $a_3(\Theta)/a_1(\Theta)$ for most angles, especially at backscattering directions. Furthermore, the ratios $b_2(\Theta)/a_1(\Theta)$ for the nonspherical and spherical quartz aerosols show significant differences at scattering angles in the range $120^\circ < \Theta < 170^\circ$. Thus our results reinforce previous indications that for most scattering angles, the phase function and the other elements of the scattering matrix for nonspherical aerosols are inadequately represented by Lorenz–Mie results computed for the same size distribution and refractive index and caution against the use of the latter in optical characterization of nonspherical particles.

The idea of compiling a synthetic phase function using a combination of experimental and theoretical Lorenz–Mie results appears to be attractive because of its simplicity and may be a useful practical tool in cases when experimental data are not available in the entire scattering angle interval from 0° to 180°. Somewhat similar procedures were described by Hill et al. [25] and Moreno et al. [26]. We have mentioned, however, that there are several issues that may make the application of this procedure less straightforward than one would like it to be. Our current research is focused on addressing the potential complexifying factors one-by-one.

Finally, we note that Mishchenko et al. [27] used the synthetic phase function to analyze the potential effect of nonsphericity on the results of retrievals of mineral tropospheric aerosols based on radiance observations from earth-orbiting satellites.

Acknowledgements

It is a pleasure to thank J.F. de Haan and W. Vassen for many fruitful discussions and two anonymous reviewers for constructive comments. This research was supported by the NASA Radiation Sciences Program managed by Donald Anderson.

References

[1] Mishchenko MI, Lacis AA, Carlson BE, Travis LD. Nonsphericity of dust-like tropospheric aerosols: implications for aerosol remote sensing and climate modeling. Geophys Res Lett 1995;22:1077–80.

[2] Krotkov NA, Flittner DE, Krueger AJ, Kostinski A, Riley C, Rose W, Torres O. Effect of particle non-sphericity on satellite monitoring of drifting volcanic ash clouds. JQSRT 1999;63:613–30.

[3] Diner DJ, Abdou WA, Bruegge CJ, Conel JE, Crean KA, Gaitley BJ, Helmlinger MC, Kahn RA, Martonchik JV, Pilorz SH, Holben BN. MISR aerosol optical depth retrievals over southern Africa during the SAFARI-2000 dry season campaign. Geophys Res Lett 2001;28:3127–30.

[4] Dubovik O, Holben B, Eck TF, Smirnov A, Kaufman YJ, King MD, Tanré D, Slutsker I. Variability of absorption and optical properties of key aerosol types observed in worldwide locations. J Atmos Sci 2002;59:590–608.

[5] Draine BT. The discrete dipole approximation for light scattering by irregular targets. In: Mishchenko MI, Hovenier JW, Travis LD, editors. Light scattering by nonspherical particles: theory, measurements, and applications. San Diego: Academic Press, 2000. p. 131–45.
[6] Lumme K. Scattering properties of interplanetary dust particles. In: Mishchenko MI, Hovenier JW, Travis LD, editors. Light scattering by nonspherical particles: theory, measurements, and applications. San Diego: Academic Press, 2000. p. 555–83.
[7] Mishchenko MI, Travis LD, Macke A. *T*-matrix method and its applications. In: Mishchenko MI, Hovenier JW, Travis LD, editors. Light scattering by nonspherical particles: theory, measurements, and applications. San Diego: Academic Press, 2000. p. 147–72.
[8] Yang P, Liou KN. Finite difference time domain method for light scattering by nonspherical and inhomogeneous particles. In: Mishchenko MI, Hovenier JW, Travis LD, editors. Light scattering by nonspherical particles: theory, measurements, and applications. San Diego: Academic Press, 2000. p. 173–221.
[9] Muinonen K. Light scattering by stochastically shaped particles. In: Mishchenko MI, Hovenier JW, Travis LD, editors. Light scattering by nonspherical particles: theory, measurements, and applications. San Diego: Academic Press, 2000. p. 323–52.
[10] Hovenier JW. Measuring scattering matrices of small particles at optical wavelengths. In: Mishchenko MI, Hovenier JW, Travis LD, editors. Light scattering by nonspherical particles: theory, measurements, and applications. San Diego: Academic Press, 2000. p. 355–65.
[11] Gustafson BÅS. Microwave analog to light-scattering measurements. In: Mishchenko MI, Hovenier JW, Travis LD, editors. Light scattering by nonspherical particles: theory, measurements, and applications. San Diego: Academic Press, 2000. p. 367–90.
[12] Volten H, Muñoz O, Rol E, de Haan JF, Vassen W, Hovenier JW, Muinonen K, Nousiainen T. Scattering matrices of mineral aerosol particles at 441.6 and 632.8 nm. J Geophys Res 2001;106:17,375–401.
[13] King MD, Kaufman YJ, Tanré D, Nakajima T. Remote sensing of tropospheric aerosols from space: past, present, and future. Bull Am Meteorol Soc 1999;80:2229–59.
[14] Billings BH, Frederikse HPR, Bleil DF, Lindsay RB, Cook RK, Marion JB, Crosswhite HM, Zemansky MW, editors. American Institute of Physics handbook. New York: McGraw-Hill, 1972. p. 6–27.
[15] Volten H. Light scattering by small planetary particles: an experimental study. PhD dissertation, Free University: Amsterdam, 2001.
[16] Hansen JE, Travis LD. Light scattering in planetary atmospheres. Space Sci Rev 1974;16:527–610.
[17] Mishchenko MI, Hovenier JW, Travis LD. Concepts, terms, notation. In: Mishchenko MI, Hovenier JW, Travis LD, editors. Light scattering by nonspherical particles: theory, measurements, and applications. San Diego: Academic Press, 2000. p. 3–27.
[18] Mishchenko MI, Dlugach JM, Yanovitskij EG, Zakharova NT. Bidirectional reflectance of flat, optically thick particulate layers: an efficient radiative transfer solution and applications to snow and soil surfaces. JQSRT 1999;63:409–32.
[19] Mishchenko MI, Travis LD, Macke A. Scattering of light by polydisperse, randomly oriented, finite circular cylinders. Appl Opt 1996;35:4927–40.
[20] Mishchenko MI, Travis LD, Kahn RA, West RA. Modeling phase functions for dustlike tropospheric aerosols using a shape mixture of randomly oriented polydisperse spheroids. J Geophys Res 1997;102:16,831–47.
[21] Hovenier JW, Volten H, Muñoz O, van der Zande WJ, Waters LBFM. Laboratory studies of scattering matrices for randomly oriented particles. Potentials problems and perspectives. JQSRT 2003, this issue.
[22] Mishchenko MI, Mackowski DW, Travis LD. Scattering of light by bispheres with touching and separated components. Appl Opt 1995;34:4589–99.
[23] Jaggard DL, Hill C, Shorthill RW, Stuart D, Glantz M, Rosswog F, Taggart B, Hammond S. Light scattering from particles of regular and irregular shape. Atmos Environ 1981;15:2511–9.
[24] Mishchenko MI, Wiscombe WJ, Hovenier JW, Travis LD. Overview of scattering by nonspherical particles. In: Mishchenko MI, Hovenier JW, Travis LD, editors. Light scattering by nonspherical particles: theory, measurements, and applications. San Diego: Academic Press, 2000. p. 29–60.
[25] Hill SC, Hill AC, Barber PW. Light scattering by size/shape distributions of soil particles and spheroids. Appl Opt 1984;23:1025–31.

[26] Moreno F, Muñoz O, López-Moreno JJ, Molina A, Ortiz JL. A Monte Carlo code to compute energy fluxes in cometary nuclei. Icarus 2002;156:474–84.
[27] Mishchenko MI, Geogdzhayev IV, Liu L, Ogren JA, Lacis AA, Rossow WB, Hovenier JW, Volten H, Muñoz O. Aerosol retrievals from AVHRR radiances: effects of particle nonsphericity and absorption and an updated long-term global climatology of aerosol properties. JQSRT 2003, this issue.